Overexpression of Soluble Fibrinogen-like Protein 2 in MSCs Ameliorates Renal Ischemia-Reperfusion Injury in Mice by Modulating Neutrophils

Guo-Shan Chen[1,2]*, Wen-Hao Xiong[1,2]*, Dan-Zhou Li[1,2]*, Peng-Hui Zhang[1,2]*, Yi-Ting Wang[1,2], Yong-Chao Zhang[1,2], Feng Qi[1,2]

[1]Department of General Surgery, Tianjin Medical University General Hospital, Tianjin, China
[2]Tianjin Key Laboratory of Precise Vascular Reconstruction and Organ Function Repair, Tianjin, China
*These authors contributed equally to this work.

Background: Renal ischemia-reperfusion (I/R) injury is a major cause of graft dysfunction and failure, driving inflammation and tissue damage. Mesenchymal stem cells (MSCs) possess therapeutic potential due to their immunomodulatory properties. Notably, neutrophils express the inhibitory receptor CD32b, which is a specific target of the immunosuppressive molecule soluble fibrinogen-like protein 2 (sFgl2).

Aims: This study aimed to investigate the therapeutic efficacy and underlying mechanisms of genetically engineered MSCs expressing sFgl2 (sFgl2-MSCs) in treating renal I/R injury, with a focus on neutrophil regulation.

Study Design: An *in vivo* renal I/R injury mouse model.

Methods: Following imaging to localize MSCs, mice were randomly allocated into four treatment groups. Treatments were administered according to group assignments. Renal function was assessed using serum creatinine and blood urea nitrogen levels, while systemic inflammation was evaluated by measuring serum interleukin-1 beta (IL-1β), interleukin (IL)-6, tumor necrosis factor-alpha (TNF-α), and IL-10 via enzyme-linked immunosorbent assay (ELISA). Neutrophil proportions in the blood and kidney were analyzed by flow cytometry. At 24 h, surface expression of CD95 and CD206 was assessed; CD206 was used to define neutrophils with N2-like (CD206$^+$) and N1-like (CD95$^+$) phenotypic features. Histopathological scoring of renal tissue was performed at 24 h.

Infiltration of Ly6G$^+$ neutrophils and citrullinated histone H3 (CitH3) as well as myeloperoxidase/CitH3 co-localization (an indicator of neutrophil extracellular traps, NETs) were detected by immunohistochemistry and immunofluorescence. Circulating free DNA (cf-DNA) in plasma was quantified using PicoGreen dye. Furthermore, the impact of sFgl2-MSCs on bone marrow-derived neutrophil polarization and function was evaluated *in vitro* using flow cytometry, ELISA, and a co-culture system.

Results: While unmodified MSCs exhibited a moderate therapeutic effect, sFgl2-MSCs treatment was significantly more effective. sFgl2-MSCs markedly improved renal function, reduced histopathological damage (e.g., tubular necrosis), and modulated systemic cytokine levels by decreasing pro-inflammatory (IL-1β, IL-6, TNF-α) and increasing anti-inflammatory (IL-10) cytokines. Crucially, sFgl2-MSCs regulated neutrophil responses in the kidney: they increased the proportion of N2-like neutrophils and decreased N1-like neutrophils, concurrently reducing NET-related markers, as evidenced by decreased CitH3 and cf-DNA. Mechanistically, sFgl2-MSCs enhanced neutrophil immunoregulatory function via the TGFβ-Smad2/3 signaling pathway.

Conclusion: Genetically modified sFgl2-MSCs alleviate renal I/R injury. This protective effect is associated with engagement of neutrophil CD32b receptors, activation of the TGFβ-Smad2/3 pathway, promotion of a protective N2-like neutrophil phenotype, and suppression of N1-like and NET-related markers.

INTRODUCTION

Renal ischemia-reperfusion (I/R) is the primary cause of acute kidney injury (AKI).[1] It can also lead to graft dysfunction, delayed recovery, and other complications, resulting in failure in renal transplantation, which seriously affects the prognosis of patients.[2] Among them, neutrophils are the key "destructors," which are activated during I/R, and the released reactive oxygen species and other substances attack renal tissue cells and aggravate the damage.[3-5] However, at present, there is a lack of efficient and specific treatment methods in clinical practice, and the mechanism of neutrophil-mediated injury is not completely clear, so it is difficult to accurately regulate its activation and function. Therefore, it is urgent to explore potential therapeutic strategies that can interfere with the key links of neutrophils in order to induce apoptosis, improve renal function, and enhance patient outcomes.

Mesenchymal stem cells (MSCs) are notable in regenerative medicine and cellular therapy for their unique biological traits and vast potential.[6] They possess remarkable abilities of self-renewal and differentiation into diverse cell lineages, along with potent immune-modulating properties. Originating from sources such as adipose tissue, bone marrow, and umbilical cords, MSCs are readily available and have earned the moniker of "superstar cells" for their exceptional potential in tissue repair. When inflammation arises, MSCs localize to the site and secrete cytokines and growth factors to regulate the immune microenvironment and reduce inflammatory damage, thus drawing significant attention for treating inflammation-related diseases.[7,8]

MSCs have great potential in the treatment of nephropathy, especially in renal I/R injury.[9] They can not only inhibit excessive immune responses by secreting anti-inflammatory cytokines but also promote angiogenesis and cell repair by secreting growth factors through paracrine action.[10] However, when MSCs are used alone to treat renal I/R injury, their function is affected by the complex injury microenvironment, and their curative effect is limited. There is an urgent need to investigate strategies aimed at boosting their immune-regulatory capabilities.

CD32b stands as the sole inhibitory Fcγ receptor, significantly contributing to innate immunity and the regulation of humoral immune responses.[11] Moreover, a deficiency in CD32b elevates susceptibility to autoimmune disorders.[12] Research has further revealed that CD32b is also expressed on neutrophils, where it exerts functional effects.[13] Soluble fibrinogen-like protein 2 (sFgl2) serves as a crucial functional ligand for CD32b.[14] As a key immunosuppressive molecule secreted by regulatory T-cells (Tregs), it serves as a central effector in mediating their regulatory functions.[15] sFgl2 has been widely utilized across various medical domains, including organ transplantation,[16] the management of inflammatory bowel disease,[17] the treatment of sepsis,[18] and in the fight against tumors and parasitic infections.[19]

MATERIALS AND METHODS

Experimental animals and ethics statement

This study was conducted in accordance with the ARRIVE guidelines 2.0. All animal procedures followed the 3R principles (Replacement, Reduction, and Refinement). Mice were monitored daily postsurgery. A predefined humane endpoint scoring system was implemented, evaluating criteria including excessive weight loss (> 20%), hypothermia, and severe lethargy. Mice reaching the endpoint criteria were euthanized promptly to minimize suffering. Six- to eight-week-old male C57BL/6J mice (20–21 g) were housed in standard ventilated cages with unrestricted access to food and water. Prior to the commencement of the experiments, they underwent a one-week acclimatization period in a temperature-regulated environment ($25 \pm 2\,°C$) with a 12-hour light/dark cycle. All animal procedures were performed in compliance with the Chinese Council on Animal Care guidelines and following protocols approved by the Animal Ethical and Welfare Committee of Tianjin Medical University General Hospital (approval number: IRB2025-DW-87, date: 18.09.2025).

Isolation of MSCs

Fat tissue was harvested from the groin area of 6–8-week-old C57BL/6J mice on day 8 under a sterile workbench. The harvested adipose tissue was placed into 15-mL centrifuge tubes (Corning, New York, USA) containing 5 mL of DMEM/F12 medium (Gibco, MA, USA). Type I collagenase (1 mg/mL; Solarbio, Beijing, China) was added to the tubes, and the samples were incubated at $37\,°C$ for 1.5 hours with continuous shaking at 200 rpm to ensure uniform digestion.

After complete digestion, the mixture was filtered through a 40-μm mesh strainer. The filtrate was centrifuged at 1500 rpm for 5 minutes to isolate the cells, and this centrifugation step was repeated twice to ensure thorough cell collection.

The isolated cells were resuspended in DMEM/F12 medium supplemented with 15% fetal bovine serum and 1% antibiotics (Solarbio, China) and plated onto 6-cm culture dishes (Corning, USA). Cultures were maintained at $37\,°C$ in a humidified incubator with 5% CO_2, and the medium was replaced every other day. By the 7th day, MSCs were obtained and used in subsequent experiments.

Transfection of MSCs with sFgl2

Second-generation MSCs were plated into 6-well culture dishes at a density of 8.0×10^4 cells per well and grown until approximately 60% confluency. A 1 mL transfection cocktail was prepared for viral-mediated gene transfer by mixing 40 μL of an enhanced protein infection reagent, 10 μL of Fgl2-overexpressing lentivirus (Ubi-MCS-3FLAG-CBh-gcGFP-IRES-puromycin, 5.0×10^8 TU/mL; Genchem, Shanghai, China), and 950 μL of DMEM/F12 medium containing 15% fetal bovine serum.

Cells were incubated with the transfection mixture at $37\,°C$ for 12 hours. After incubation, the transfection medium was aspirated and replaced with complete culture medium. Three days after medium replacement, stable transfected MSCs (sFgl2-MSCs) were selected

using 2 μg/mL puromycin (Solarbio, Beijing, China). Both the cells and their corresponding supernatants were used for subsequent experimental procedures.

Animal models and therapeutic experiments

Bilateral I/R injury was induced in mice under inhalation anesthesia as described previously.[20] Briefly, microaneurysm clips were applied to clamp both renal pedicles for 40 minutes, after which the clips were removed to restore blood flow. Kidney color changes were observed to confirm reperfusion before closing the incisions. A sham operation, in which the kidneys were exposed without clamping, was also performed. A rectal probe connected to a heating pad was used to maintain body temperature within the range of 36.6 °C–37.2 °C.

To minimize bias, a computer-generated random sequence was used to assign ear-tagged mice to four groups: Sham, I/R+PBS, I/R+MSCs, and I/R+sFgl2-MSCs, with six mice per group. Allocation concealment was achieved by having an independent technician prepare the corresponding treatments (MSCs or sFgl2-MSCs) suspended in 150 μL PBS at 1×10^6 cells/mouse, or PBS vehicle, according to the concealed randomization list. This ensured that the surgeons performing the procedures and the personnel administering the tail vein injections were blinded to group identity. Treatments were administered at the onset of reperfusion.

Mice were euthanized by cervical dislocation at 6, 24, and 72 hours post-reperfusion. Kidneys and blood samples were promptly collected. Kidney tissues intended for histopathological analysis were fixed in 10% buffered formalin. Blinding was maintained throughout the outcome assessment and data processing phases. Specifically, researchers performing histological scoring, flow cytometry data acquisition/gating, enzyme-linked immunosorbent assay (ELISA) plate reading, and initial statistical analyses were unaware of group allocation. Blinding was only lifted after the completion of all quantitative analyses and generation of initial results. All results were cross-validated by at least two independent researchers.

Monitoring of MSCs in vivo

To investigate the homing capability of MSCs to inflammatory sites, in vivo near-infrared (NIR) fluorescence imaging was performed. MSCs were labeled in vitro with the lipophilic fluorescent dye DiR (excitation/emission: 748/780 nm; Thermo Fisher, USA) according to the manufacturer's protocol. DiR-labeled MSCs (1×10^6 cells in 100 μL PBS per mouse) were administered via tail vein injection. Mice were euthanized 12 hours post-injection, and major organs (lungs and kidneys) were harvested for imaging.

Imaging and quantitative analysis: all ex vivo organs were imaged using an IVIS Spectrum system coupled with Living Image® software. Quantitative analysis was performed in a single-blinded manner (the analyst was unaware of the experimental groups). The specific workflow was as follows: within the image analysis module of the software, regions of interest (ROIs) of consistent shape and size were manually drawn to encompass each entire organ. The software automatically calculated the total radiant efficiency [reported as average radiant efficiency in units of $(p/s/cm^2/sr) / (μW/cm^2)$] for each ROI.

To subtract background signals, an identically sized ROI was drawn in an adjacent tissue-free area of the same image, and its signal value was defined as the background. The net fluorescence intensity for each organ was calculated as follows: net fluorescence = organ ROI signal − background ROI signal. To assess the relative enrichment of MSCs in the injured kidney, the kidney-to-lung fluorescence ratio (kidney net fluorescence intensity/lung net fluorescence intensity) was further calculated for each mouse. This ratio was used for subsequent intergroup statistical analyses.

Renal function and histological assessment

Serum creatinine (sCr) and blood urea nitrogen (BUN) levels were measured using commercial spectrophotometric kits. For histopathological analysis, kidney tissue samples were fixed in 10% buffered formalin, paraffin-embedded, and sectioned. Sections were stained with hematoxylin and eosin (H&E). A standardized semiquantitative scoring system was applied to evaluate renal tubular injury. The scoring was based on the percentage of cortical tubules exhibiting pathological features, including tubular epithelial cell necrosis or detachment, tubular dilation, and cast formation.[21] The injury score for each field was assigned as follows: 0, no lesion; 1, < 10%; 2, 10–25%; 3, 26–50%; 4, 51–75%; and 5, > 75% involvement. To minimize bias, all histological scoring was performed by two independent pathologists who were blinded to group allocation. For each kidney, ten random, non-overlapping cortical fields (100 × magnification) were evaluated. The final score for each animal was calculated as the average of the scores from all fields assessed by both observers.

Flow cytometry

Antibody staining and flow cytometry were performed following previously reported protocols.[22] Cell staining and flow cytometry analysis were conducted according to a predefined, stepwise gating strategy to ensure consistency and reproducibility. All antibodies were titrated prior to use, and fluorescence-minus-one controls were included to establish accurate gates.

To characterize MSC phenotype, third-passage MSCs were harvested and stained with a panel of antibodies, including anti-CD29 (APC), anti-CD44 (PE), anti-CD45 (APC), anti-CD34 (APC), and anti-SCA-1 (APC), all sourced from eBioscience (USA). To assess the impact of MSCs on neutrophil phenotype, neutrophils that had been co-cultured with various MSC groups were collected, resuspended, and stained with antibodies, including anti-Ly6G (FITC), anti-CD95 (PE), anti-CD206 (APC), and anti-CD32b (PE).

To assess neutrophil differentiation in whole blood, red blood cells were removed and the remaining cells were stained with anti-Ly6G (FITC), anti-CD11b (PerCP-Cyanine 5.5), anti-CD95 (PE), and anti-CD206 (APC), following the manufacturer's guidelines.

To prevent non-specific staining arising from dead cells, viability dye (Zombie APC-Cyanine 7) was used to differentiate live cells from dead cells. Unless specified otherwise, all antibodies for flow

cytometry were procured from BioLegend (USA). The proportion of immune cells with different phenotypes was analyzed using FlowJo software.

Single cells were first gated on forward scatter area versus forward scatter height to exclude doublets and aggregates. Live cells were further gated based on viability dye negativity. For *in vivo* blood samples, live single cells were gated as CD11b$^+$ Ly6G$^+$ cells to identify neutrophils, whereas for *in vitro* co-cultured bone marrow-derived neutrophils (BMDNs), Ly6G$^+$ cells from live single cells were directly defined as neutrophils. Within the gated neutrophil population, the expression of CD95 and CD206 was observed to quantify N1-like (Ly6G$^+$CD95$^+$) and N2-like (Ly6G$^+$CD206$^+$) phenotypes, and CD32b expression was analyzed similarly.

Immunofluorescence

Renal neutrophil infiltration was evaluated by immunofluorescence. After removal, kidneys were fixed in 10% buffered formalin, processed for paraffin embedding, and sectioned at 3 μm. Sections were permeabilized with 0.2% Triton X-100 in PBS, blocked with 10% goat serum, and incubated overnight with primary antibodies against myeloperoxidase (MPO; 1:200) and citrullinated histone H3 (CitH3; 1:200), both obtained from Proteintech (China). Fluorescently conjugated secondary antibodies were then applied. To ensure that each animal was treated as a single statistical unit, positive cells were counted in five random, non-overlapping fields (100 ×) per sample, and the average of these counts was used as that animal's single data point for intergroup comparison, thereby avoiding pseudoreplication.

Immunofluorescence was also used to assess indicators of neutrophil extracellular trap (NET) formation after *in vitro* co-culture. Neutrophils from each group were seeded on poly-L-lysine-coated coverslips and fixed with 4% paraformaldehyde for 15–20 minutes at room temperature. Cells were permeabilized with 0.2% Triton X-100 in PBS for 10–15 minutes and blocked with 5% BSA. SYTOX Green dye was applied according to the kit instructions and incubated in the dark at room temperature for 15–30 minutes. Subsequently, the samples were examined under a fluorescence microscope. For antibody staining, rabbit anti-mouse MPO (1:200) and rabbit anti-mouse CitH3 (1:200) primary antibodies (Proteintech, China) were applied, followed by appropriate secondary antibodies according to the manufacturer's instructions. The samples were counterstained with DAPI and examined under a fluorescence microscope. Positive cells were counted in five random, non-overlapping fields (100 ×) per sample, and the average of these counts was used as the single data point for each animal to ensure accurate intergroup comparison, thereby avoiding pseudoreplication.

Immunohistochemical staining

Ly6G$^+$ neutrophils and CitH3$^+$ cells in renal tissue were detected using a streptavidin-biotin peroxidase complex method. Kidney sections were immunostained with primary antibodies against Ly6G (1:2000; Abclonal, China) and CitH3 (1:400; Proteintech, China). Quantification was performed with strict measures to avoid pseudoreplication and ensure objectivity. Two independent pathologists, blinded to group allocation, counted positively stained cells. For each kidney section, five non-overlapping fields were randomly selected from the renal cortex at 40 × magnification. The counts from these five fields were averaged to yield a single mean value per animal, which served as the independent statistical unit (n = 1). The final result for each sample was the mean of the counts obtained from the two observers.

Bone marrow-derived neutrophils were isolated and co-cultured with MSCs

Neutrophils were purified from C57BL/6 bone marrow-derived cells using Ly6G microbeads (Miltenyi Biotec) and co-cultured with MSCs according to previous reports. The inflammatory response was simulated under the conditions described above using 100 ng/mL LPS. A total of 1×10^6 neutrophils were inoculated into the upper chamber of a 0.4-μm transwell. In the lower chamber, the following groups were added: PBS, 1×10^5 MSCs, 1×10^5 sFgl2-MSCs, 1×10^5 sFgl2-MSCs + anti-CD32b (15 μg/mL), and 1×10^5 sFgl2-MSCs + BI-4659 (1 μM). After 24 hours of co-culture, the percentages of Ly6G$^+$CD95$^+$ and Ly6G$^+$CD206$^+$ cells in BMDNs were analyzed by flow cytometry.

Measurement of cell-free DNA concentration

Blood samples anticoagulated with heparin were collected from each group. Samples were centrifuged and stored at −80 °C until analysis. Plasma DNA was quantified according to the manufacturer's instructions using the Quant-iT™ PicoGreen double-stranded DNA detection kit. Fluorescence intensity was measured with a microplate reader, reflecting the amount of PicoGreen-bound double-stranded DNA. DNA concentration was determined using a standard curve generated from Lambda DNA standards (100 μg/mL) supplied by the manufacturer.

Enzyme-linked immunosorbent assay (ELISA)

For *in vivo* experiments, whole blood was collected from mice and centrifuged at 4 °C, 1000 × g for 20 minutes to isolate serum. For *in vitro* experiments, supernatants from neutrophils in different treatment groups were harvested and centrifuged under the same conditions to remove debris. Levels of interleukin-1 beta (IL-1β), interleukin (IL)-6, tumor necrosis factor-alpha (TNF-α), and IL-10 in serum and supernatants were measured using ELISA kits (Abclonal, Wuhan, China) according to the manufacturer's instructions with a microplate reader. To assess sFgl2 secretion by sFgl2-MSCs, supernatants from each MSC group were collected, centrifuged at 4 °C and 1000 × g for 20 minutes, and analyzed using a commercial ELISA kit (Uscn Life Sciences, Wuhan, China) according to the manufacturer's instructions.

Western blotting

Protein samples were extracted from neutrophils and kidney tissue in the co-culture system using RIPA lysis buffer (R0010, Solarbio) supplemented with protease and phosphatase inhibitors (P1261, Solarbio). The lysates were separated by SDS-PAGE and transferred onto a PVDF membrane (0.45 μm, Millipore). After blocking with 5% BSA in TBST for 2 hours, the membrane was incubated overnight

at 4 °C with the following primary antibodies: anti-MPO (1:1000; Proteintech), anti-CitH3 (1:1000; Proteintech), anti-PAD4 (1:1000; Proteintech), anti-Smad2/3 (1:1000; CST), anti-phospho-Smad2/3 (1:1000; CST), and anti-GAPDH (1:3000; Affinity). Protein bands were visualized using an ECL substrate and imaged.

Statistical analysis

All *in vitro* experiments were independently repeated three times. *In vivo* data were acquired from six mice per group. Graphing and statistical analyses were performed using GraphPad Prism v.9.5.0 (GraphPad Software). Data are presented as the mean ± standard deviation (SD). The Shapiro–Wilk test was used to assess the normality of continuous variables, and the Brown-Forsythe test was used to assess homogeneity of variances. Unpaired two-tailed Student's t-tests were used for comparisons between two groups. For comparisons among multiple groups under a single condition, one-way ANOVA followed by Tukey's post-hoc test was employed.

For cross-sectional analysis of *in vivo* data collected at multiple time points (e.g., plasma levels of BUN, Scr, cf-DNA, and peripheral blood neutrophil proportion measured at 6, 24, and 72 hours in independent animal cohorts), a two-way ANOVA was used to analyze the effects of treatment and time. This analysis assessed the main effects of the treatment factor, the time factor, and their interaction. When a statistically significant interaction was detected, indicating that treatment effects differed across time points, Tukey's post-hoc test was performed to compare specific group differences within each individual time point.

A post-hoc power analysis was conducted for the primary outcome (serum sCr at 24 hours post-I/R), specifically comparing the I/R + MSCs vs. I/R + sFgl2-MSCs groups. The effect size (Cohen's d) was calculated from the observed mean difference (23.77) and pooled SD (11.58), resulting in a Cohen's d of 2.05. With an alpha level of 0.05 and a sample size of n = 6 per group, the achieved statistical power for this comparison was ∼ 98%, indicating sufficient statistical reliability for the main conclusion. Detailed post-hoc power calculations for secondary outcomes and exploratory *in vitro* experiments are provided in Supplementary Table 1. A *p* value of < 0.05 was considered statistically significant.

Multiple comparisons and family-wise error rate control

To manage the increased risk of false positives due to multiple testing, a tiered analytical strategy was employed. First, sCr at 24 hours post-I/R was prespecified as the primary outcome, with the significance threshold set at α = 0.05 and verified by post-hoc power analysis. Second, BUN, plasma cf-DNA levels, and peripheral blood neutrophil proportion at 24 hours were prespecified as key secondary outcomes to support the primary finding, interpreted in conjunction with effect size estimates and biological plausibility. Finally, measurements at other time points (6 and 72 hours), *in vitro* mechanistic assays, and analyses of multiple cytokines and protein markers were considered exploratory, aiming to generate hypotheses and elucidate potential mechanisms rather than provide confirmatory evidence.

For all pairwise comparisons, two-way ANOVA followed by Tukey's test was used for correction. The robustness of findings was further evaluated by emphasizing the magnitude of effect sizes, biological coherence, and consistency across related metrics.

RESULTS

Characterization of MSCs

MSCs were extracted from mouse inguinal fat and characterized based on their phenotypic markers. Flow cytometry analysis (Figure 1a) showed that MSCs highly expressed CD44 (97.7%), CD29 (99.5%), and SCA-1 (99.7%), while minimally expressing CD45 (0.51%) and CD34 (0.97%), consistent with typical MSC phenotypic characteristics. Morphologically, the cells were spindle-shaped and closely arranged (Figure 1b).

Based on the high-purity MSC population, a lentiviral transfection system was constructed to generate sFgl2 gene-modified MSCs (sFgl2-MSCs). ELISA of the culture supernatant demonstrated high-level sFgl2 secretion (*p* < 0.001, Figure 1c), confirming successful lentiviral transfection.

After co-culture with mouse BMDN, flow cytometry analysis (Figures 1d and e) revealed that CD32b expression on neutrophils in the sFgl2-MSC group was markedly elevated compared to both the control and normal MSC groups. Western blot analysis further confirmed this finding (Figures 1f and 1g). These results indicate that MSCs can induce CD32b expression in neutrophils, and sFgl2 transfection significantly enhances this effect. Overall, a functional MSC system with elevated sFgl2 expression was successfully established, providing a basis for subsequent functional studies.

sFgl2-MSCs reduce renal I/R injury, neutrophil proportion, and NET-related markers in mice

To assess MSC homing to injured tissue, their biodistribution was evaluated using *ex vivo* NIR fluorescence imaging. DiR-labeled MSCs were administered intravenously to sham-operated mice and mice with renal I/R injury. Organs were harvested 12 hours later for imaging and quantitative analysis (Figure 2a). In sham mice, fluorescence signals were predominantly detected in the brain and lungs. In contrast, mice subjected to renal I/R exhibited significantly stronger fluorescence in the kidneys, indicating preferential accumulation of MSCs in ischemic kidneys.

Blood and tissue samples were collected from independent cohorts of mice at 6, 24, and 72 hours post-I/R. At 24 and 72 hours after renal I/R, MSC administration led to a notable decline in sCr (Figure 2c) and BUN levels (Figure 2b) compared to untreated mice. Furthermore, sFgl2-MSCs provided additional protection beyond MSC therapy alone. Notably, at 6 hours post-I/R, neither MSCs nor sFgl2-MSCs produced a statistically significant improvement in renal function.
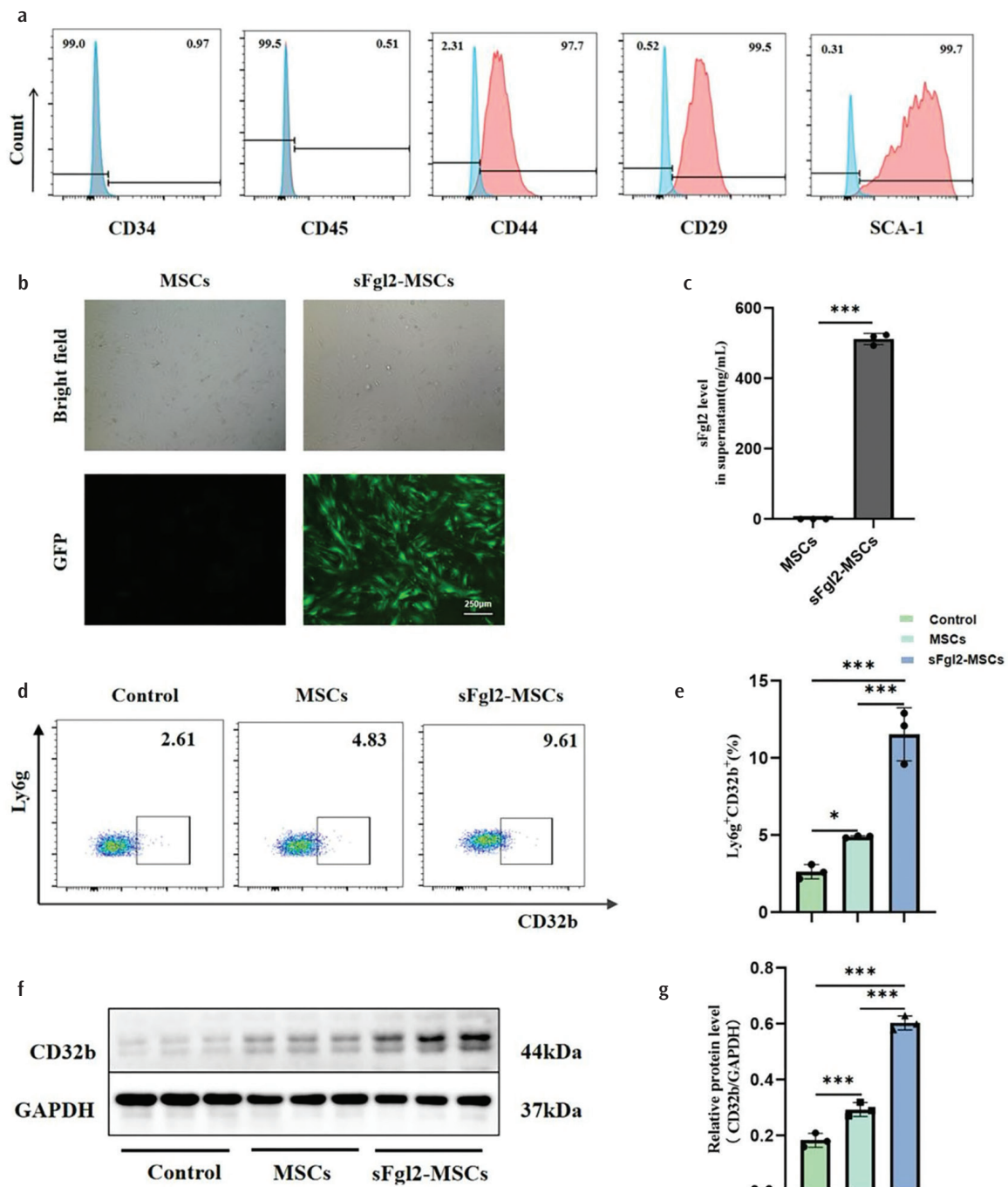
FIG. 1. Characterization of MSCs. (a) Flow cytometry was employed to identify the surface markers of MSCs, encompassing positive markers (CD44, CD29, and SCA-1) and negative markers (CD34 and CD45). (b) The morphological features of MSCs and sFgl2-MSCs at the third passage were observed (scale bar: 250 μm). The successful transfection was evidenced by the expression of green fluorescent protein. (c) The concentration of sFgl2 in the culture supernatants of both MSCs and sFgl2-MSCs was measured using an ELISA (n = 3 independent experiments). (d and e) Representative flow cytometry plots and corresponding statistical charts illustrate the expression levels of CD32b in BMDNs that were co-cultured with either genetically modified or unmodified MSCs (n = 3 independent experiments). (f and g) The expression levels of CD32b on BMDNs that were co-cultured with either genetically modified or unmodified MSCs were assessed via WB analysis, with a sample size of n = 3 independent experiments. Data are presented as the mean ± standard deviation. Statistical significance was determined using unpaired t-test (two groups) or one-way ANOVA followed by Tukey's test (multiple groups), as detailed in Methods. n.s., $p > 0.05$, *$p < 0.05$, **$p < 0.01$, and ***$p < 0.001$. MSCs, mesenchymal stem cells; ELISA, enzyme-linked immunosorbent assay; BMDNs, bone marrow-derived neutrophils; sFgl2, soluble fibrinogen-like protein 2.
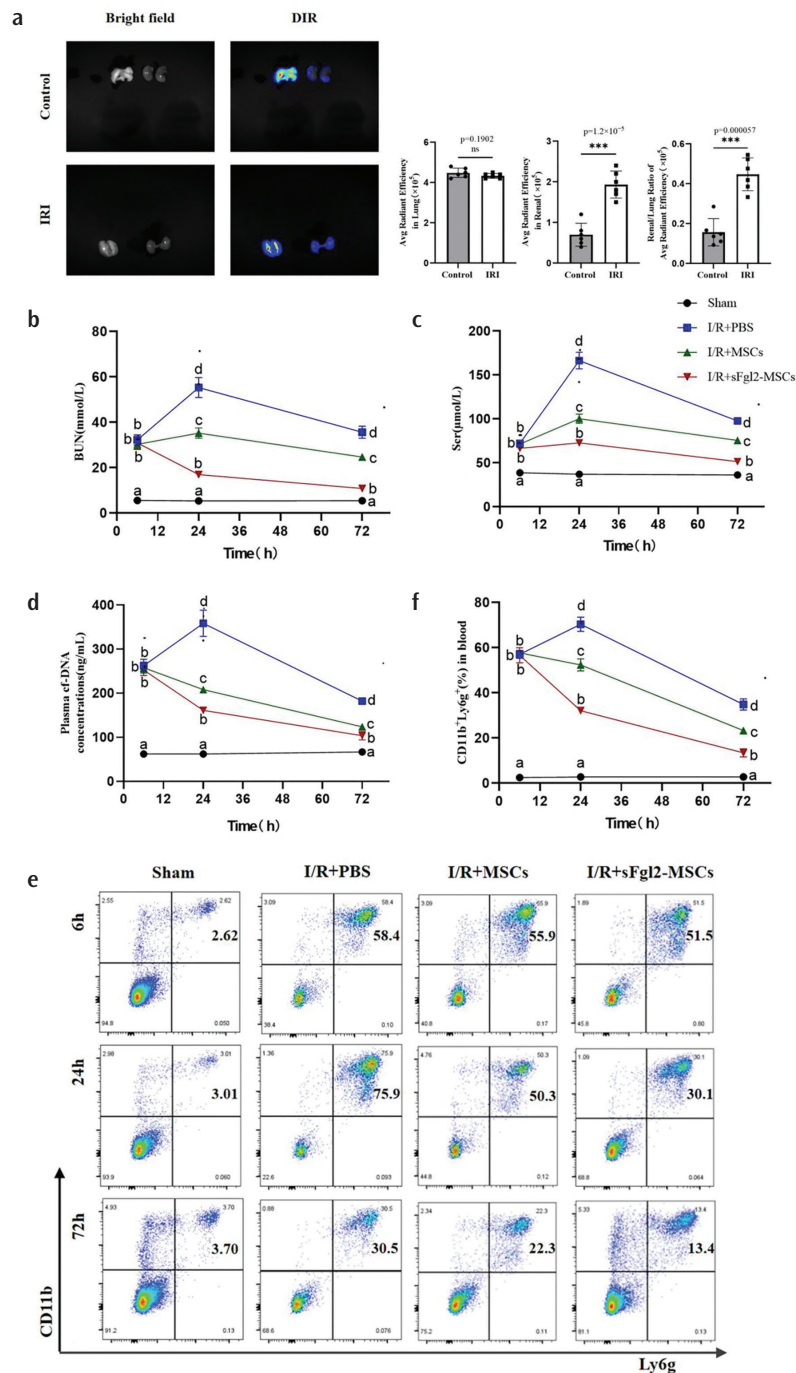
FIG. 2. Effects of sFgl2-MSCs on renal I/R injury (a) biodistribution of DiR-labeled MSCs at 12 h. Representative *ex vivo* NIRF images (left) and quantitative analysis of net fluorescence intensity in lungs and kidneys after background subtraction. The kidney-to-lung ratio is shown (right). (b-d) Renal function (sCr, BUN) and a NET-related marker (plasma cf-DNA) were assessed in independent cohorts of mice at 6, 24, and 72 hours post-I/R (n = 6 mice per group per time point). (e and f) Flow cytometry analysis of CD11b$^+$ Ly6g$^+$ cells in peripheral blood at 6, 24, and 72 hours after renal I/R in different groups (n = 6 mice per group per time point). Data are mean $\pm$ standard deviation. Statistical comparisons were performed using unpaired two-tailed t-test (for two groups) or two-way ANOVA followed by Tukey's post-hoc test (for multiple groups across time). Different letters indicate statistically significant differences among groups at the same time point ($p < 0.05$). A significant interaction between treatment and time was observed, indicating that the renoprotective effects of MSCs and sFgl2-MSCs varied over time.as detailed in Methods. n.s., $p > 0.05$, *$p < 0.05$, **$p < 0.01$, and ***$p < 0.001$. MSCs, mesenchymal stem cells; sFgl2, soluble fibrinogen-like protein 2; sCr, serum creatinine; BUN, blood urea nitrogen;I/R, ischemia-reperfusion; NET, neutrophil extracellular trap.

To comprehensively evaluate the effects of sFgl2-MSCs, blood indices were dynamically monitored at 6, 24, and 72 hours post-reperfusion, and changes in neutrophil proportion and plasma cf-DNA levels were systematically analyzed to assess neutrophil activation and its correlation with tissue injury. The proportion of blood neutrophils peaked at 24 hours post-I/R (Figure 2d), and plasma cf-DNA levels were highest at this time point (Figures 2e and 2f), indicating strong neutrophil activation and extracellular DNA release. MSC treatment reduced both neutrophil proportion and plasma cf-DNA levels, while sFgl2-MSCs further enhanced these effects. At 72 hours post-I/R, sFgl2-MSC treatment continued to reduce neutrophil proportion and cf-DNA levels. At 6 hours post-I/R, neither MSCs nor sFgl2-MSCs significantly affected neutrophil proportion or cf-DNA levels. Collectively, these findings suggest that sFgl2 enhances the therapeutic effects of MSCs in reducing neutrophil activation and NET-related markers during renal I/R injury.

sFgl2-MSCs attenuate renal I/R injury by limiting neutrophil infiltration. Favoring N2-like polarization and reducing NET-related markers at 24 hours

Neutrophils are pivotal mediators of renal I/R injury.[23] Our time-course analysis pinpointed 24 hours post-reperfusion as a critical window: it represented the peak of systemic neutrophil activation and NET-associated damage (indicated by the highest levels of circulating neutrophils and plasma cf-DNA; Figures 2d-f), which coincided with the onset of significant therapeutic effects for both MSCs and sFgl2-MSCs (evidenced by significant reductions in sCr and BUN; Figures 2b, c). Therefore, to mechanistically dissect how sFgl2-MSCs modulate renal injury, we focused our study on subsequent histopathological and phenotypic analyses at this 24-hour time point, allowing for a comprehensive assessment of renal tissue damage, neutrophil infiltration, and phenotype within the most representative period of active injury and treatment response.

H&E staining (Figure 3a) revealed that the untreated group suffered from severe tubular necrosis, accompanied by the detachment of renal tubular epithelial cells. In contrast to the untreated group, the MSC-treated group displayed a marked reduction in the extent of tubular necrosis. Particularly, when compared to the MSC-treated group, the sFgl2-MSC-treated group exhibited an even more pronounced decrease in the severity of renal tubular necrosis.

Moreover, flow cytometry analysis revealed that MSC administration led to a decreased proportion of N1-like neutrophils and an increased proportion of N2-like neutrophils in the bloodstream. Treatment with sFgl2-MSCs not only replicated this effect but further shifted neutrophil polarization toward an N2-like phenotype, demonstrating the capacity to alter neutrophil phenotypes (Figures 3d, e).

Subsequently, to investigate neutrophil infiltration and indicatrs of NET formation in renal tissue, immunohistochemistry was utilized to assess the expression of Ly6G and CitH3 at 24 hours post-I/R. As shown in Figures 3b and c, MSC treatment decreased renal Ly6G+ and CitH3+ cells compared to the untreated group. This reduction was further amplified by sFgl2-MSC treatment.

Furthermore, immunofluorescence co-localization analysis of CitH3 (a histone marker associated with NETs) and MPO (a neutrophil marker) was performed (Figure 3f). The fluorescence signals for both CitH3 and MPO were lower in the MSC-treated group than in the untreated controls. Again, sFgl2-MSC treatment induced a more pronounced decrease in these signals. Collectively, these findings suggest that sFgl2 enhances the capacity of MSCs to limit neutrophil infiltration and reduce the presence of NET-associated markers in injured kidneys.

sFgl2 MSCs lowered pro-inflammatory and raised anti—inflammatory factor levels in the serum

To evaluate the regulatory effects of different MSC treatments on inflammatory responses in I/R injury, this study employed ELISA to quantitatively measure serum inflammatory cytokine levels in mice. The results revealed that, in comparison to the untreated group, the —MSC-treated group demonstrated reduced expression of pro-inflammatory cytokines, namely IL-1β (Figure 3g), IL-6 (Figure 3h), and TNF-α (Figure 3i), while showing elevated levels of the anti-inflammatory cytokine IL-10 (Figure 3j).

When compared to the —MSC-treated group, the sFgl2-MSC-treated group— exhibited even more pronounced decreases in the expression of IL-1β, IL-6, and TNF-α, along with a further surge in IL-10 levels. To summarize, MSC treatment markedly lowered the serum concentrations of the pro—inflammatory Cytokines IL-6, TNF-α, and IL-1β, while boosting the level of the anti-inflammatory cytokine IL-10 in mice with the I/R model. Notably, sFgl2-MSCs demonstrated a more robust anti-inflammatory impact.

sFgl2 activates Smad2/3, promotes MSC-driven N2-like neutrophil polarization, and suppresses inflammation

We established that sFgl2-overexpressing MSCs promote an N2-like neutrophil phenotype and mitigate renal I/R injury. We next asked whether sFgl2-MSCs could similarly influence BMDNs in an *in vitro* inflammatory setting. Flow cytometry analysis of co-cultured BMDNs (Figures 4a, b) showed that MSCs alone increased the Percentage of N2-like neutrophils and decreased that of N1-like neutrophils compared with the control. Notably, sFgl2-MSCs produced a more pronounced shift, further elevating the proportion of N2-like cells and reducing N1-like cells. This enhanced effect was abrogated by CD32b blockade.

Furthermore, sFgl2-MSCs downregulated neutrophil-derived pro-inflammatory cytokines (IL-6, TNF-α, IL-1β) while promoting anti-inflammatory IL-10 secretion (Figures 4f-i). Collectively, these results indicate that sFgl2 augments the ability of MSCs to induce. An immunosuppressive shift in neutrophils, characterized by an increased proportion of Ly6G+CD206+ N2-like neutrophils, coupled with suppressed production of pro-inflammatory cytokines and enhanced secretion of IL-10.

To evaluate the indicators of NET formation, BMDNs after co-culture were analyzed using SYTOX Green staining (Figure 4c) and MPO/CitH3 co-localization (Figure 4e). The results revealed that MSC treatment led to a decline in neutrophil-derived extracellular DNA release and downregulation of MPO and CitH3 expression.
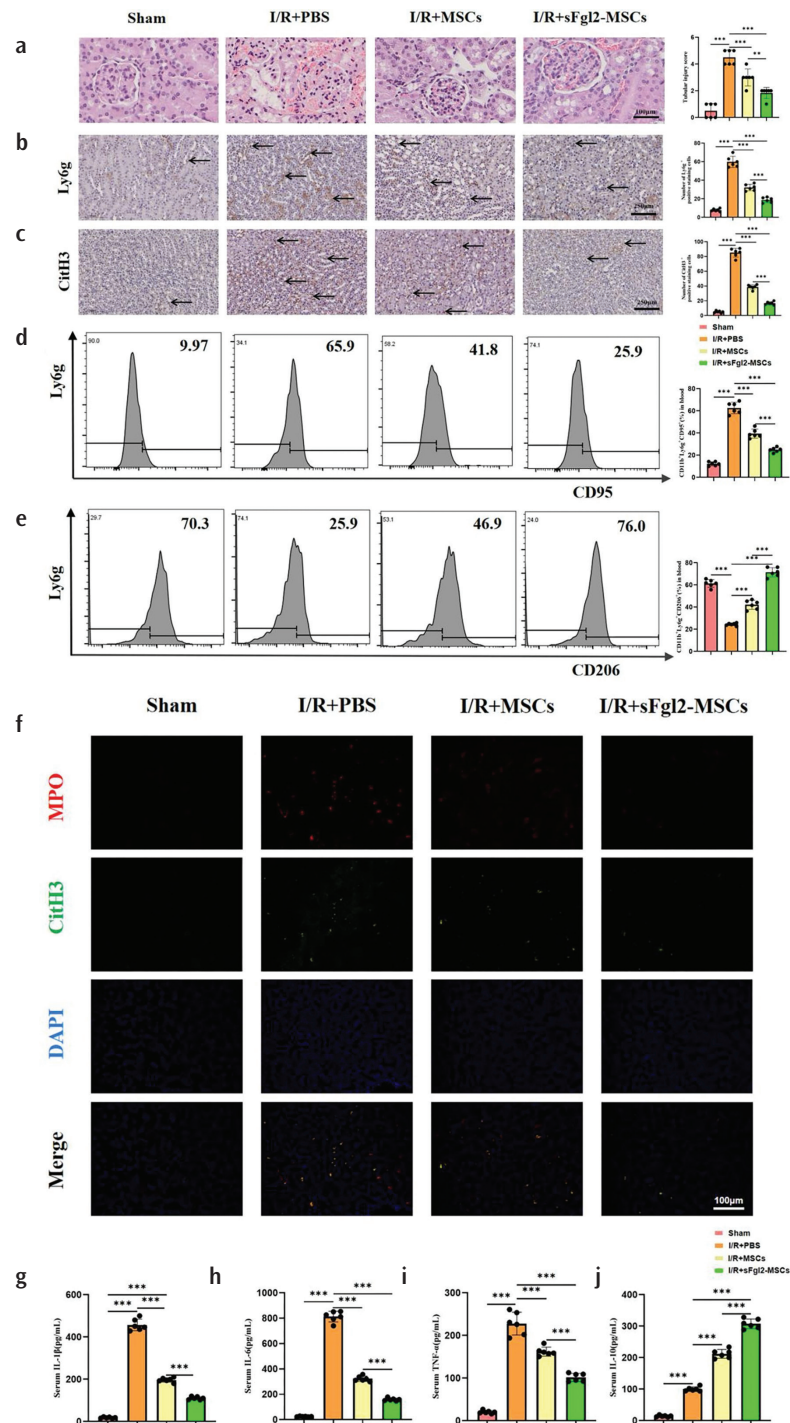
FIG. 3. sFgl2-MSCs at 24 h post-renal I/R reduce kidney damage, promote an N2-like neutrophil phenotype, and suppress NETs-associated markers. (a) Representative H&E-stained kidney sections. Tubular injury was scored (0-5) as detailed in Methods (n = 6 mice per group). (b and c) Representative images and quantification of Ly6G+ and CitH3+ cells. Positive cells (arrows) were counted in five random cortical fields (40 x) per sample, and the average per animal is plotted (n = 6 mice per group). Scale bars are shown. (d and e) The representative histograms and statistical graphs for Ly6g+ CD95+ and Ly6g+ CD206+ neutrophils in the blood are also shown (n = 6 mice per group). (f) Representative immunofluorescence images showing MPO (green), CitH3 (red), and DAPI (blue) staining as an indicator of NETs. (g-j) The levels of proinflammatory cytokines interleukin-1 beta (IL-1β), interleukin (IL)-6, and TNF-α, along with the anti-inflammatory cytokine IL-10, in the serum were measured via ELISA, with a sample size of n = 6 mice per group. Data are mean ± standard deviation. Statistical comparisons were performed using one-way ANOVA followed by Tukey's post-hoc test (for multiple groups), as detailed in Methods. n.s., $p > 0.05$, *$p < 0.05$, **$p < 0.01$, and ***$p < 0.001$. MSCs, mesenchymal stem cells; sFgl2, soluble fibrinogen-like protein 2; H&E, hematoxylin and eosin; MPO, myeloperoxidase; CitH3, citrullinated histone H3; NETs, neutrophil extracellular traps; ELISA, enzyme-linked immunosorbent assay; TNF-α, tumor necrosis factor-alpha; I/R, ischemia-reperfusion.
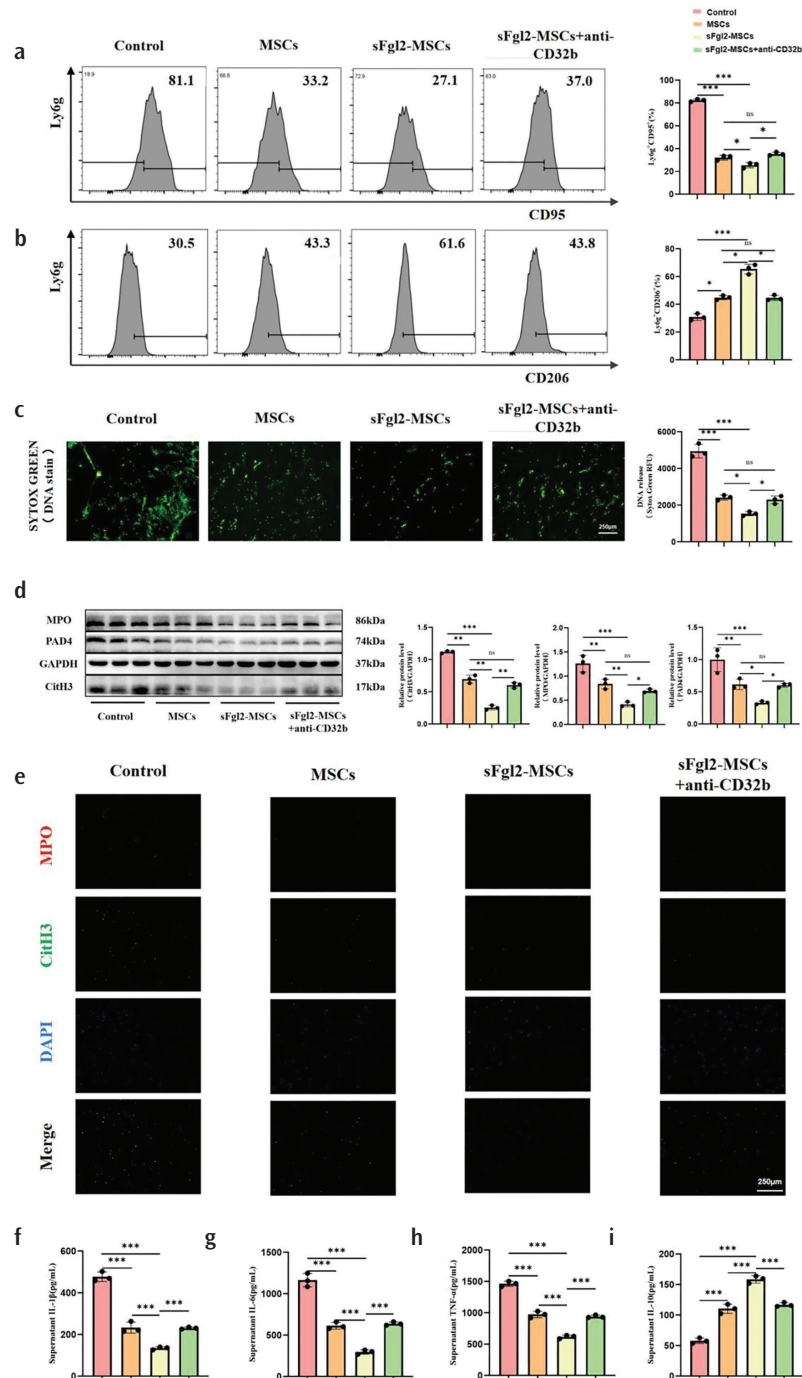
FIG. 4. sFgl2 in MSCs promotes an N2-like phenotype in BMDNs and enhances anti-inflammatory effects. (a, b) Representative histograms and statistical plots depicting Ly6g$^+$CD95$^+$ and Ly6g$^+$CD206$^+$ BMDNs in the coculture system are displayed (n = 3 independent experiments). (c) Extracellular DNA release (as an indicator of NETs) was assessed by Sytox Green staining, and fluorescence intensity was quantified (n = 3). (d) The protein levels of MPO, PAD4, and CitH3 in BMDNs were determined via WB, with GAPDH serving as an internal control for normalization across diverse treatment conditions. Statistical analyses were carried out on the calculated ratios of MPO/GAPDH, PAD4/GAPDH, and CitH3/GAPDH (n = 3 independent experiments). (e) The levels of MPO and CitH3 were detected by immunofluorescence. (f-i) The levels of the pro-inflammatory cytokines TNF-α, interleukin (IL)-6, and IL-1 beta (IL-1β), along with the anti - inflammatory cytokine IL-10, in the culture supernatant were measured using the ELISA method (n = 3 independent experiments). Data are mean ± standard deviation. Statistical comparisons were performed using one-way ANOVA followed by Tukey's post-hoc test (for multiple groups), as detailed in Methods. n.s., $p > 0.05$, *$p < 0.05$, **$p < 0.01$, and ***$p < 0.001$. MSCs, mesenchymal stem cells; sFgl2, soluble fibrinogen-like protein 2; NETs, neutrophil extracellular traps; BMDNs, bone marrow-derived neutrophils; MPO, myeloperoxidase; CitH3, citrullinated histone H3; ELISA, enzyme-linked immunosorbent assay; TNF-α, tumor necrosis factor-alpha.

Notably, sFgl2-MSCs exhibited an even more pronounced effect, further decreasing neutrophil extracellular DNA release and suppressing MPO and CitH3 expression. This enhancement effect was reversed by blocking CD32b. Western blot results once again verified this conclusion (Figure 4d). In summary, sFgl2 can enhance the ability of MSCs to suppress NET-associated processes through CD32b.

Prior research findings have indicated that the TGF-β-Smad2/3 signaling cascade occupies a pivotal position in the regulation of myeloid cell differentiation and immune polarization processes.[24,25] Therefore, it is assumed that the TGF-β-Smad2/3 pathway is responsible for the regulation of MSCs on neutrophils. In order to determine whether and how MSCs in different treatment groups affect expression or activation of the TGF-β-Smad2/3 pathway in BMDNs, we performed WB detection (Figure 5a). The findings demonstrated that treatment with MSCs led to a marked elevation in the levels of TGF-β1 and p-Smad2/3 within BMDNs. Moreover, when compared to the group receiving MSC treatment alone, the group treated with sFgl2-MSCs exhibited a further significant increase in the expression of TGF-β1 and p-Smad2/3. However, this additional upregulation was effectively counteracted by the blockade of CD32b.

To verify the functional involvement of this pathway, we employed the TGF-β type I receptor inhibitor BI-4659. This inhibitor significantly suppresses the kinase activity of TGF-βRI, thereby markedly reducing the phosphorylation of downstream Smad2/3 without affecting TGF-β1 expression itself. Results showed that BI-4659 treatment did not alter TGF-β1 levels but significantly attenuated the activation of p-Smad2/3 induced by sFgl2-MSCs (Figure 6e). Flow cytometry analysis further indicated that inhibition of the TGF-β-Smad2/3 pathway markedly impaired the ability of sFgl2-MSCs to promote neutrophil polarization toward an N2-like phenotype while suppressing their shift toward an N1-like phenotype (Figures 6a, b). Correspondingly, the suppressive effects of sFgl2-MSCs on neutrophil extracellular DNA release and on the expression of PAD4 and CitH3 were significantly reduced upon inhibition of the TGF-β-Smad2/3 pathway (Figure 6d). Furthermore, the capacity of sFgl2-MSCs to downregulate neutrophil-derived pro-inflammatory cytokines (IL-6, TNF-α, IL-1β) and to enhance the secretion of anti-inflammatory cytokine IL-10 was likewise diminished following BI-4659-mediated inhibition of the TGF-β-Smad2/3 pathway (Figures 6f-i).

Based on these results, we propose that, compared with MSCs, sFgl2-MSCs exert more potent immunosuppressive effects by activating the Smad2/3 pathway via CD32b, thereby promoting an N2-like neutrophil phenotype and suppressing NET-associated processes.

DISCUSSION

Surgical renal ischemia and inadequate renal perfusion are the primary etiologies of AKI.[26] During reperfusion, the innate immune system is activated by damage-associated molecular patterns released following the initial injury. As the first responders, neutrophils migrate to the injured site along chemokine gradients. They inflict direct oxidative damage on renal tubular structures via the release of reactive oxygen species and significantly exacerbate secondary injury through mechanisms such as the formation of NETs.[27]

Stem cell therapy has garnered considerable attention in regenerative medicine. Substantial preclinical and clinical evidence supports the potential of stem cell-based therapeutic approaches as a key strategy for AKI.[28,29] MSCs are particularly notable for their capacity to modulate the differentiation and activation of diverse immune cell subsets, including T-cells, macrophages, and dendritic cells. Their favorable *in vitro* characteristics—easy culture, expansion, and preservation—further enhance their therapeutic appeal. Given these potent immunomodulatory properties, MSCs have been investigated for the treatment of renal I/R injury.[30] However, the efficacy of unmodified MSCs alone remains suboptimal, necessitating further strategies to augment their immunoregulatory functions.
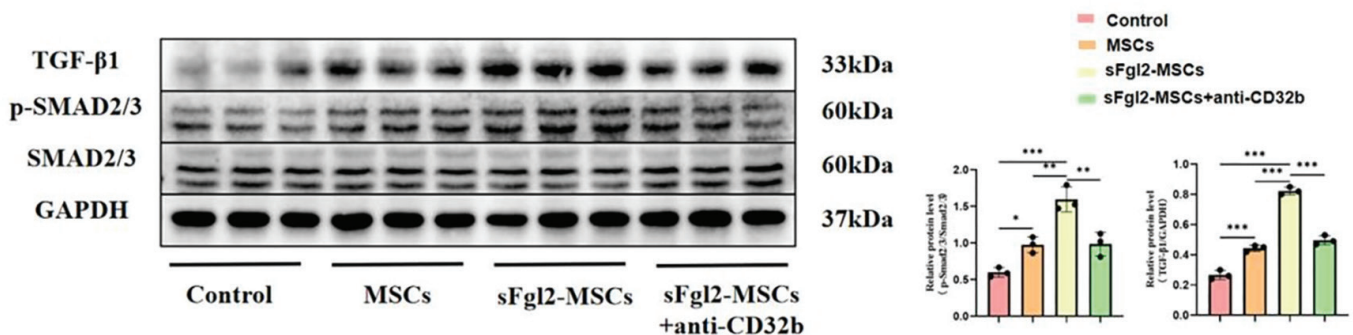
FIG. 5. sFgl2 amplified MSCs' immunosuppression on BMDNs via TGF-β -Smad2/3 pathway. (a) In BMDNs undergoing various treatment conditions, WB was carried out to detect the protein levels of TGF-β1, p-Smad2/3, and Smad2/3, using GAPDH as an internal reference. (n = 3 independent experiments). Data are mean ± standard deviation. Statistical comparisons were performed using one-way ANOVA followed by Tukey's post- hoc test (for multiple groups), as detailed in Methods. n.s., $p > 0.05$, *$p < 0.05$, **$p < 0.01$, and ***$p < 0.001$. MSCs, mesenchymal stem cells; sFgl2, soluble fibrinogen-like protein 2; BMDNs, bone marrow-derived neutrophils.
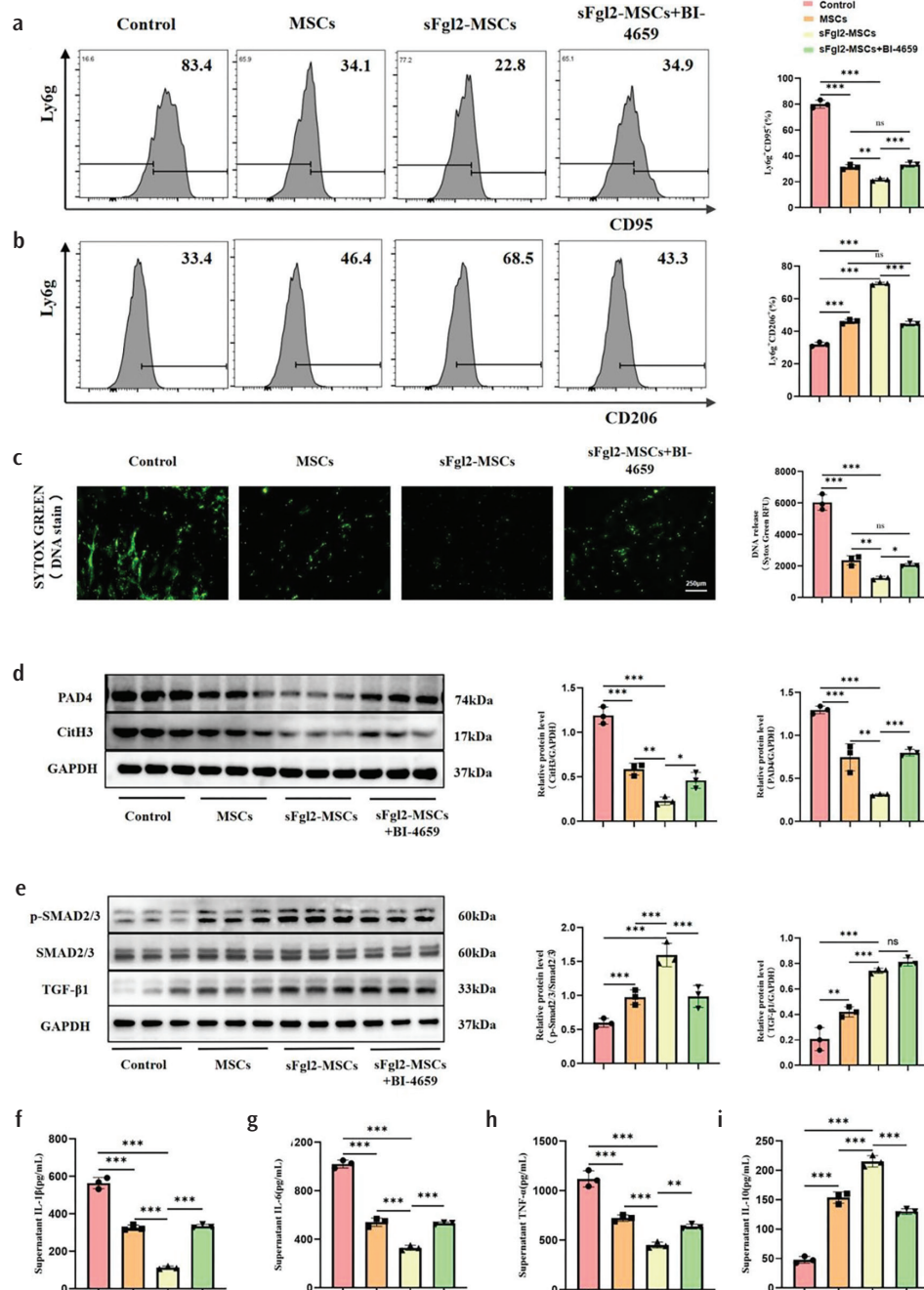
FIG. 6. sFgl2 in MSCs promotes an N2-like, anti-inflammatory phenotype in BMDNs via the TGF-β-Smad2/3 pathway. (a, b) Representative histograms and statistical plots depicting Ly6g+CD95+ and Ly6g+CD206+BMDNs in the coculture system are displayed (n = 3 independent experiments). (c) Extracellular DNA release (as an indicator of NETs) was assessed by Sytox Green staining, and fluorescence intensity was quantified (n = 3). (d) The protein levels of PAD4, and CitH3 in BMDNs were determined via WB, with GAPDH serving as an internal control for normalization across diverse treatment conditions. Statistical analyses were carried out on the calculated ratios of PAD4/GAPDH, and CitH3/GAPDH (n = 3 independent experiments). (e) In BMDNs undergoing various treatment conditions, WB was carried out to detect the protein levels of TGF-β1, p-Smad2/3, and Smad2/3, using GAPDH as an internal reference. (n = 3 independent experiments). (f-i) The levels of the pro - inflammatory cytokines TNF-α, interleukin (IL)-6, and IL-1β, along with the anti - inflammatory cytokine IL-10, in the culture supernatant were measured using the ELISA method (n = 3 independent experiments). Data are mean ± standard deviation. Statistical comparisons were performed using one-way ANOVA followed by Tukey's post-hoc test (for multiple groups), as detailed in Methods. n.s., $p > 0.05$, $*p < 0.05$, $**p < 0.01$, and $***p < 0.001$. MSCs, mesenchymal stem cells; sFgl2, soluble fibrinogen-like protein 2; BMDNs, bone marrow-derived neutrophils; NETs, neutrophil extracellular traps; CitH3, citrullinated histone H3; ELISA, enzyme-linked immunosorbent assay; TNF-α, tumor necrosis factor-alpha.

A common approach to enhance MSC function involves genetic modification to overexpress relevant immunomodulatory factors. In this study, we employed lentiviral transduction to engineer MSCs for high-level secretion of the sFgl2. It is critical to distinguish sFgl2 from its membrane-bound counterpart, mFgl2. While mFgl2 possesses direct prothrombinase activity and can influence coagulation, sFgl2 functions primarily as an anticoagulant immunomodulator—a key effector molecule of regulatory T-cells—and lacks procoagulant activity. Our strategy was designed to harness this specific immunomodulatory function.

Our *in vitro* co-culture experiments demonstrated that MSCs could upregulate CD32b expression on BMDNs. This was accompanied by a shift in neutrophil phenotypic balance, characterized by an expansion of the N2-like (CD206+) population, a contraction of the N1-like (CD95+) population, and a reduction in NET-related markers. These effects were significantly potentiated by sFgl2-MSCs. Collectively, these findings indicate that sFgl2 enhances the ability of MSCs to induce CD32b expression, suppress NET formation, and promote a neutrophil phenotype skewed toward the N2-like state.

We propose a mechanism by which sFgl2-MSCs exert enhanced modulation of neutrophil phenotype and NET-associated processes via the p-SMAD2/3 pathway. CD32b contains an immunoreceptor tyrosine-based inhibitory motif domain,[31] known to influence downstream Smad2/3 activation.[32] Consistent with this, our data demonstrate that the presence of sFgl2 upregulates p-Smad2/3 levels, whereas blockade of CD32b diminishes them. Notably, specific inhibition of the Smad2/3 pathway using the TGFβRI inhibitor BI-4659 significantly abrogated the enhanced ability of sFgl2-MSCs to promote polarization of BMDNs toward an N2-like anti-inflammatory phenotype. Taken together, these findings suggest that the augmented immunomodulatory capacity of sFgl2-MSCs is mediated, at least in part, through the efficient activation of the Smad2/3 signaling cascade, initiated by the engagement of sFgl2 with CD32b.

Previous studies indicate that systemically administered MSCs initially accumulate in the lungs, with a subset subsequently migrating to the sites of injury.[33] Our *in vivo* imaging findings align with this paradigm, confirming significant pulmonary localization while also detecting a meaningful signal in injured kidneys, confirming successful delivery of a portion of cells to the target organ. Functionally, compared to conventional MSCs, sFgl2-MSC administration at 24 and 72 hours post-I/R resulted in superior preservation of renal architecture and a more favorable outcome, including a pronounced reduction in circulating neutrophils and a stronger shift toward an N2-like phenotype, alongside diminished NET-related markers and more effective amelioration of renal dysfunction (sCr and BUN).

Notably, neither treatment was effective at the 6-hour time point, likely due to the time required for MSC homing and paracrine factor accumulation. The rationale for focusing our subsequent detailed histopathological and phenotypic analyses on the 24-hour time point was twofold, grounded in our kinetic data. First, 24 hours post-reperfusion represented the peak of systemic neutrophil recruitment and NET-associated injury, as evidenced by maximal levels of circulating neutrophils and plasma cf-DNA (Figures 2d-f). Second, this peak injury window coincided precisely with the onset of significant therapeutic efficacy for both MSC types, marked by significant declines in sCr and BUN (Figures 2b, c). Therefore, to most effectively capture and dissect the modulatory effects of sFgl2-MSCs on neutrophil-driven pathology, we concentrated our evaluations on this critical 24-hour period.

At this peak injury phase, sFgl2-MSCs uniquely promoted N2-like reprogramming of circulating neutrophils while concurrently suppressing the release of NET-associated markers, demonstrating superior multifaceted control over the mouse neutrophil response. At the molecular level, they more effectively downregulated pro-inflammatory cytokines (IL-6, IL-1β, TNF-α) and upregulated the anti-inflammatory cytokine IL-10. This precise immunomodulation—curtailing destructive inflammation while promoting reparative pathways—resolves the apparent paradox wherein an "immunosuppressive" molecule confers protection. In the context of acute I/R, where tissue damage is driven by excessive inflammation, sFgl2 acts not to induce global immunosuppression but to restore immune homeostasis, which is ultimately cytoprotective. This concept is supported by evidence that endogenous sFgl2 upregulation is associated with the recovery phase in ischemia-reperfusion injury (IRI),[34] suggesting that our therapeutic strategy amplifies natural resolution-facilitating mechanisms.

This study has limitations that must be considered and inform future directions. First, several methodological constraints temper the interpretation of our findings. We acknowledge the lack of an a priori power analysis, which underscores the necessity of prestudy statistical calculations in future work to confirm effect sizes. Our histological quantification, while focused on the predominantly injured renal cortex at the 24-hour peak of injury, did not separately assess the medulla, leaving potential regional differences unexplored. Furthermore, our assessment of NETosis relies on histological markers (CitH3/MPO), which, while widely accepted, provide indirect evidence; future studies employing direct methodologies such as extracellular DNA imaging would strengthen these conclusions. The primary mechanistic focus on the 24-hour post-I/R time point, chosen as the critical window of neutrophil-driven injury and initial MSC efficacy, limits insights into the dynamics of this immunomodulation at later repair phases.

Second, our interpretation of neutrophil polarization is constrained by the current conceptual framework. While the operational terms "N1-like" and "N2-like" are used to denote pro-inflammatory and anti-inflammatory states, respectively, we acknowledge that this dichotomy represents a simplified model of neutrophil heterogeneity. Our classification relies on a limited set of surface

markers (CD95 and CD206) and lacks accompanying functional assays or transcriptional validation to fully define these subsets. This framework, although useful for hypothesis generation, remains an area of active debate within the field. Future studies incorporating multidimensional phenotyping are required to more precisely characterize the phenotypic shift induced by sFgl2-MSCs.

Third, key biological mechanisms remain to be fully elucidated. The complete signaling cascade linking CD32b engagement to Smad2/3 activation warrants deeper investigation. Beyond neutrophils, a systematic evaluation of the impact of sFgl2-MSCs on other immune cell populations (e.g., macrophages and T-cells) within the renal microenvironment is needed to understand the broader therapeutic landscape. Finally, the distinct roles of the secreted form (sFgl2) and

the membrane-bound isoform (mFgl2), and their potential interplay with coagulation pathways in IRI, remain important questions for future investigation. Addressing these limitations will be central to our subsequent studies, which will incorporate robust experimental design and explore these specific pathways and broader immune interactions to advance the translational development of sFgl2-MSCs.

This study provides evidence that engineered sFgl2-MSCs can target neutrophil CD32b receptors and activate the TGFβ-Smad2/3 pathway *in vitro* (Figure 7). These actions are correlated with a shift in neutrophil phenotypes from a pro-inflammatory N1-like toward a reparative N2-like state and alleviation of renal I/R injury *in vivo*.
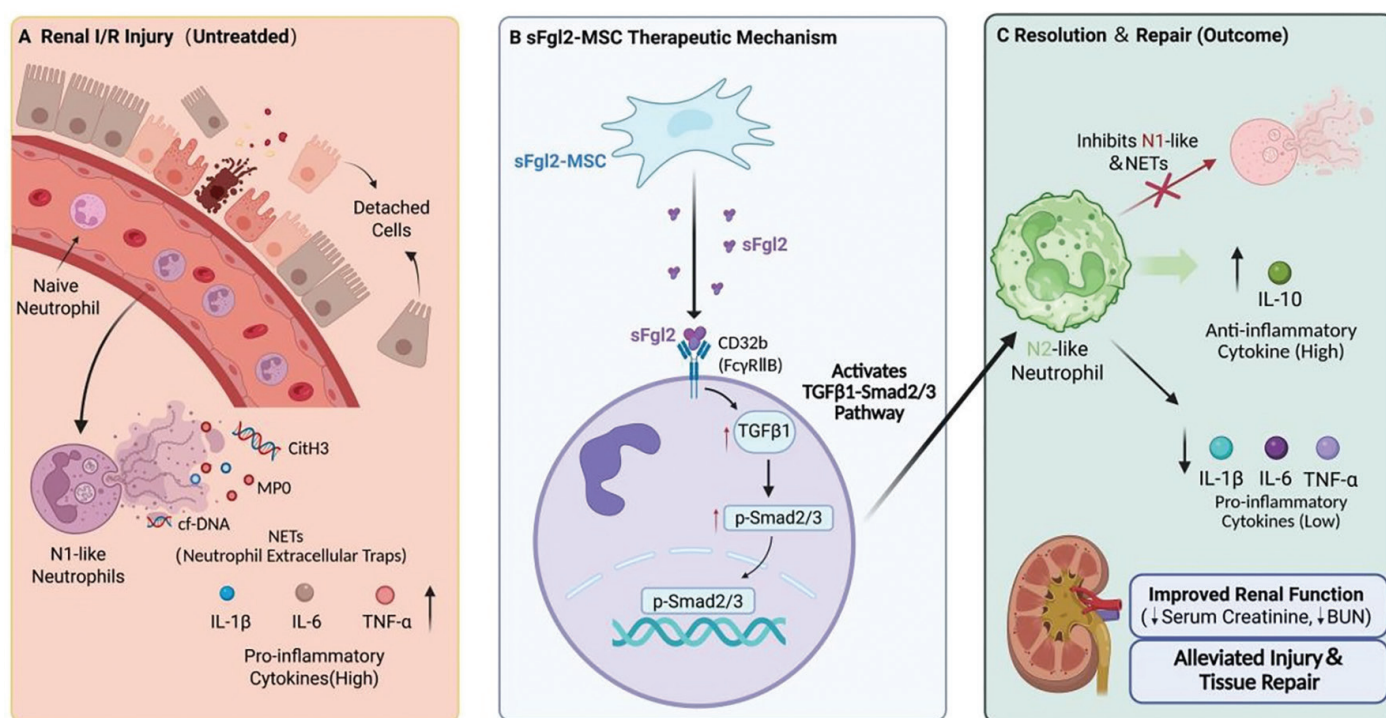
FIG. 7. sFgl2 from sFgl2-MSCs binds neutrophil CD32b, activating the TGF- β-Smad2/3 pathway. This promotes an N- to N2-like phenotypic shift, modulates NETs-associated processes, and fosters renal repair. MSCs, mesenchymal stem cells; sFgl2, soluble fibrinogen-like protein 2; MPO, myeloperoxidase; I/R, ischemia-reperfusion; CitH3,citrullinated histone H3; IL-1β, interleukin-1 beta; IL-6, interleukin-6; TNF-α, tumor necrosis factor-alpha.

REFERENCES

1. Leng J, Zhao W, Guo J, et al. E-prostanoid 3 receptor deficiency on myeloid cells protects against ischemic acute kidney injury via breaking the auto-amplification loop of necroinflammation. *Kidney Int.* 2023;103:100-114. [CrossRef]

2. Yang W, Li X, He L, et al. Empagliflozin improves renal ischemia-reperfusion injury by reducing inflammation and enhancing mitochondrial fusion through AMPK-OPA1 pathway promotion. *Cell Mol Biol Lett.* 2023;28:42. [CrossRef]

3. Wu J, Zhang F, Zheng X, et al. Identification of renal ischemia reperfusion injury subtypes and predictive strategies for delayed graft function and graft survival based on neutrophil extracellular trap-related genes. *Front Immunol.* 2022;13:1047367. [CrossRef]

4. Zhang J, Li Q, Zou YR, et al. HMGB1-TLR4-IL-23-IL-17A axis accelerates renal ischemia-reperfusion injury via the recruitment and migration of neutrophils. *Int Immunopharmacol.* 2021;94:107433. Erratum in: *Int Immunopharmacol.* 2021;97:107573. [CrossRef]

5. Wu X, You D, Pan M, et al. Knockout of the C3a receptor protects against renal ischemia reperfusion injury by reduction of NETs formation. *Cell Mol Life Sci.* 2023;80:322. [CrossRef]

6. Yao L, Hu X, Dai K, et al. Mesenchymal stromal cells: promising treatment for liver cirrhosis. *Stem Cell Res Ther.* 2022;13:308. [CrossRef]

7. Wang Y, Fang J, Liu B, Shao C, Shi Y. Reciprocal regulation of mesenchymal stem cells and immune responses. *Cell Stem Cell.* 2022;29:1515-1530. [CrossRef]

8. Liu J, Gao J, Liang Z, et al. Mesenchymal stem cells and their microenvironment. *Stem Cell Res Ther.* 2022;13:429. [CrossRef]

9. Wang Y, Ding Y, Dong H, Wuren T, Luo P. MSCs in acute kidney injury treatment: modulating mitochondrial function and inhibiting pyroptosis via PGC-1α. *Exp Cell Res.* 2025;450:114583. [CrossRef]

10. Hu H, Zou C. Mesenchymal stem cells in renal ischemia-reperfusion injury: biological and therapeutic perspectives. *Curr Stem Cell Res Ther.* 2017;12:183-187. [CrossRef]

11. Simpson AP, Oldham RJ, Cox KL, et al. FcγRIIB (CD32B) antibodies enhance immune responses through activating FcγRs. *Clin Exp Immunol.* 2025;219:uxaf015. [CrossRef]

12. Williams EL, Tutt AL, French RR, et al. Development and characterisation of monoclonal antibodies specific for the murine inhibitory FcγRIIB (CD32B). *Eur J Immunol.* 2012;42:2109-2120. [CrossRef]

13. Zhou Y, Lei J, Xie Q, et al. Fibrinogen-like protein 2 controls sepsis catabasis by interacting with resolvin Dp5. *Sci Adv.* 2019;5:eaax0629. [CrossRef]

14. Chen GS, Ji WB, Zhang BT, Xiong WH, Qi F. MSC-derived exosomes carrying sFgl2 alleviate acute rejection of mouse heart transplantation by regulating macrophage polarization. *Int Immunopharmacol.* 2025;167:115678. [CrossRef]

15. Liu XG, Liu Y, Chen F. Soluble fibrinogen like protein 2 (sFGL2), the novel effector molecule for immunoregulation. *Oncotarget.* 2017;8:3711-3723. [CrossRef]

16. Zhang Y, Yang M, Liu K, et al. sFGL2 as a potential immunosuppressive biomarker associated with COVID-19 severity in kidney transplant recipients. *Immun Inflamm Dis.* 2025;13:e70296. [CrossRef]

17. Zhu Y, Zhou J, Feng Y, et al. Control of intestinal inflammation, colitis-associated tumorigenesis, and macrophage polarization by fibrinogen-like protein 2. *Front Immunol.* 2018;9:87. [CrossRef]

18. Yang Y, Chen J, Yang J, et al. Predictive value of soluble fibrinogen-like protein 2 for survival in traumatic patients with sepsis. *Clin Chim Acta.* 2020;510:196-202. [CrossRef]

19. Galpin KJC, Rodriguez GM, Maranda V, et al. FGL2 promotes tumour growth and attenuates infiltration of activated immune cells in melanoma and ovarian cancer models. *Sci Rep.* 2024;14:787. [CrossRef]

20. Ramesh G, Ranganathan P. Mouse models and methods for studying human disease, acute kidney injury (AKI). *Methods Mol Biol.* 2014;1194:421-436. [CrossRef]

21. Wang Y, Quan F, Cao Q, et al. Quercetin alleviates acute kidney injury by inhibiting ferroptosis. *J Adv Res.* 2020;28:231-243. [CrossRef]

22. Ye K, Lan X, Wang G, et al. B7-H1 Expression is required for human endometrial regenerative cells in the prevention of transplant vasculopathy in mice. *Stem Cells Int.* 2018;2018:2405698. [CrossRef]

23. Deng X, Zhou C, Liao R, et al. Separated parabiont reveals the fate and lifespan of peripheral-derived immune cells in normal and ischaemia-induced injured kidneys. *Open Biol.* 2021;11:200340. [CrossRef]

24. Qin F, Liu X, Chen J, et al. Anti-TGF-β attenuates tumor growth via polarization of tumor associated neutrophils towards an anti-tumor phenotype in colorectal cancer. *J Cancer.* 2020;11:2580-2592. [CrossRef]

25. Fei C, Shen X, Wan L, et al. Silencing of SMAD family member 3 promotes M2 polarization of macrophages and the expression of SMAD7 in rheumatoid arthritis. *Chinese Journal of Cellular and Molecular Immunology*. 2023;39:904-909. [CrossRef]

26. Tammaro A, Kers J, Scantlebery AML, Florquin S. Metabolic flexibility and innate immunity in renal ischemia reperfusion injury: the fine balance between adaptive repair and tissue degeneration. *Front Immunol*. 2020;11:1346. [CrossRef]

27. Fu Y, Wang W, Gong N, et al. Neutrophil and neutrophil extracellular traps in acute kidney injury: from mechanisms to treatments. *Front Immunol.* 2025;16:1688207. [CrossRef]

28. Rosenberg ME. Cell-based therapies in kidney disease. *Kidney Int Suppl (2011)*. 2013;3:364-367. [CrossRef]

29. Zhuang K, Wang W, Xu C, et al. MSCs-derived HGF alleviates senescence after AKI by modulating mitoSTAT3-controlled copper flux and respiration. *Stem Cell Res Ther.* 2025;16:526. [CrossRef]

30. Lee KW, Kim TM, Kim KS, et al. Renal ischemia-reperfusion injury in a diabetic monkey model and therapeutic testing of human bone marrow-derived mesenchymal stem cells. *J Diabetes Res.* 2018;2018:5182606. [CrossRef]

31. Simpson AP, Roghanian A, Oldham RJ, et al. FcγRIIB controls antibody-mediated target cell depletion by ITIM-independent mechanisms. *Cell Rep.* 2022;40:111099. [CrossRef]

32. Tang PM, Zhang YY, Hung JS, et al. DPP4/CD32b/NF-κB circuit: a novel druggable target for inhibiting CRP-driven diabetic nephropathy. *Mol Ther.* 2021;29:365-375. [CrossRef]

33. Ji W, Wang W, Li P, et al. sFgl2 gene-modified MSCs regulate the differentiation of CD4+ T cells in the treatment of autoimmune hepatitis. *Stem Cell Res Ther*. 2023;14:316. [CrossRef]

34. Zhao Z, Yang C, Li L, et al. Increased peripheral and local soluble FGL2 in the recovery of renal ischemia reperfusion injury in a porcine kidney auto-transplantation model. *J Transl Med.* 2014;12:53. [CrossRef]